

Combinatorial optimization solving by coherent Ising machines based on spiking neural networks

Bo Lu

School of Artificial Intelligence, Beijing Normal University, Beijing 100875, China

Yong-Pan Gao

School of Electronics Engineering, Beijing University of Posts and Telecommunications, Beijing 100876, China

Kai Wen

Beijing QBoson Quantum Technology Co., Ltd., Beijing 100015, China

Chuan Wang*

School of Artificial Intelligence, Beijing Normal University, Beijing 100875, China

(Dated: August 17, 2022)

Spiking neural network is a kind of neuromorphic computing which is believed to improve on the level of intelligence and provide advantages for quantum computing. In this work, we address this issue by designing an optical spiking neural network and prove that it can be used to accelerate the speed of computation, especially on the combinatorial optimization problems. Here the spiking neural network is constructed by the antisymmetrically coupled degenerate optical parametric oscillator pulses and dissipative pulses. A nonlinear transfer function is chosen to mitigate amplitude inhomogeneities and destabilize the resulting local minima according to the dynamical behavior of spiking neurons. It is numerically proved that the spiking neural network-coherent Ising machines has excellent performance on combinatorial optimization problems, for which is expected to offer a new applications for neural computing and optical computing.

I. INTRODUCTION

Combinatorial optimization problems are of great importance in various fields of computer science. During the past decades, they are ubiquitous in various field, such as the drug design [1], financial management [2], and circuit design [3]. Due to the rapid growth of the computing power, the computation time of these problems on conventional computers tends to increase exponentially with the size of the problem due to the explosion in the number of combinations [4]. The problem in the complexity class NP could be formulated as an Ising problem with only polynomial overhead, and the loss functions can be mapped to the Ising model to complete the search from the initial state to the ground state, which has been implemented by several physical systems such as quantum annealing [5, 6], optical oscillators [7], nanomagnetic-net arrays [8, 9].

Among them, oscillator-based coherent Ising machines (CIM) are widely studied due to the advantages [10] of high speed, programmability, and parallel search. Each Ising spin in the CIM can be encoded as the phase ϕ_i of the light pulse in an optical mode. Employing the degenerate optical parametric oscillation, the phase values are enforced as the binary spin values as $\phi_i = 0, \pi$. During computation, the optical gain yields oscillation of the pluses either in-phase or out-of-phase with respective to the pump light. Meanwhile, the oscillators are coupled

with tunable coupling constant to form a network. The oscillation network can be implemented by various ways, such as the optical oscillators [11–15], opto-electronic oscillators [16, 17], spatial phase modulators [18–20], and integrated photonic chips [21].

As a quantum heuristic algorithm, CIM has excellent performance on small-scale combinatorial optimization problems [7, 10, 13], but on large-scale problems, an important technicality would arise in the model which is that the amplitude of the oscillators are not equal. This phenomenon is usually call the amplitude heterogeneity which prevents CIM from being correctly mapped to the Ising model [22], as shown in Fig.1(a). The spin configuration of the ground state of the Ising model differs from that of the CIM. During the calculation of CIM, the energy will be frozen in the excited state of the Ising model, as shown in Fig.1(b). To address the problem of amplitude heterogeneity, there are several method to fix these problem by adding a feedback mechanism to reduce the inequality of the amplitude, such as the additional uncorrelated driving signals [22], nonlinear functions [23, 24] and correcting the amplitude by the error signal [25–27].

In addition, we turn our attention to the spiking neural network (SNN) which has been simulated on the CIM based on the DOPOs neural network, and the collective behavior of neural clusters has been studied [28]. The spiking neurons which are a special type of neurons which performs the signal processing in the brain. They are considered as the next generation of neural architectures, and have been extensively studied in artificial intelligence recently [29–31]. For example, it can imitate the biolog-

* wangchuan@bnu.edu.cn

ical nervous system to produce more intelligent systems, such as brain-like learning [32, 33].

In this work, we propose a new architecture of CIM, based on a spiking neuron network composed of DOPO pulses and dissipative pulses. We find that it is able to achieve the amplitude heterogeneity and also freeze in local minima during computing for combinatorial optimization problems. By controlling the dissipative parameters of spiking neurons composed of antisymmetrically coupled DOPO and dissipative pulses, the rate and direction of contraction of the phase space volumes can be controlled to bring the system out of the frozen state. More generally, we prove the existence of neurons are similar to the dynamic behavior of class-II neurons. A SNN-CIM algorithm is proposed to achieve the instability of the local minimum by adjusting the parameters, and the performance is compared with the algorithm that only uses the nonlinear filter function. The results show that SNN-CIM has excellent performance and has more potential on complex graph structures.

II. RESULTS

A. SNN-CIM model

The model of SNN-CIM we use can be summarized in Fig.1(c). The system with correction of amplitude heterogeneity can be implemented using a CIM with a measurement-and-feedback (MFB) structure composed of DOPO pulses. The qubits for computing are represented by the optical SNN pulses which propagate cyclically in the fiber-ring cavity. For each SNN pulses, it can be divided into two types of pulses by controlling the pump, one is generated by the optical parametric oscillation with nonlinear gain process. It corresponds to the case where the pump is turned on, denoted as x , and the other pulse is the injected optical pulse with a dissipative process only, corresponding to the case where the pump is turned off, denoted as k .

A spiking neuron consists of both a type- x pulse and a type- k pulse coupled to each other with coupling strengths of J_{xk} and J_{kx} ($J_{kx} = -J_{xk}$), respectively. The spiking neurons can be connected to each other, as shown in Fig.1(d). Based on this principle, the dynamical behavior of the i th neuron can be expressed as:

$$\begin{aligned} \frac{dx_i}{dt} &= \alpha x_i - x_i^3 + J_{xk}\beta k_i + I_{ext}, \\ \frac{dk_i}{dt} &= -\beta k_i + J_{kx}x_i, \\ I_{ext} &= \tanh(\epsilon \sum_j J_{ij}x_j). \end{aligned} \quad (1)$$

where x_i is in-phase components of DOPO amplitudes, (k_i) is dissipative pulse amplitude. α denotes the nonlinear gain generated by the pump, and β is the inherent dissipation of the system. J_{ij} represents the connection between the i th and the j th neuron, and ϵ is the strength of interaction.

For the case of the power above the threshold, the DOPO pulses undergo spontaneous symmetry breaking. Then, the potential energies of the spiking neurons can be represented by the positive and negative amplitudes of the type- x pulses. According to the constraints of the combinatorial optimization problems, the connection of the neurons in the neural network can be regarded as an Ising model that evolves a spin configuration into the ground state.

B. The dynamics of the spiking neurons

According to Eq.(1), we find the dynamic properties of a spiking neuron depends on the linear stability of its fixed point. And the fixed points under steady-state solution of Eq.(1) should satisfy the relation as:

$$\begin{aligned} k_i &= \frac{1}{\beta}x_i, \\ 0 &= (\alpha - 1)x_i - x_i^3 + I_{ext}. \end{aligned} \quad (2)$$

The solution satisfying Eq.(2) is denoted as x_0 and the linear stability of a fixed point ($x_0, x_0/\beta$) can be obtained by the eigenvalues of its Jacobian matrix:

$$J_i = \begin{bmatrix} \alpha - 3x_0^2 & -\beta \\ 1 & -\beta \end{bmatrix}. \quad (3)$$

Here the eigenvalues λ_i^\pm of the Jacobian matrix are given as follows:

$$\lambda_i^\pm = \frac{1}{2}(T \pm \sqrt{T^2 - 4\Delta}), \quad (4)$$

where Δ and T are the determinant and trace of the Jacobian matrix, respectively. Then, we have $\Delta = J_{xx}J_{kk} - J_{xk}J_{kx} = (3x_0^2 - \alpha + 1)\beta$ and $T = J_{xx} + J_{kk} = \alpha - 3x_0^2 - \beta$. Numerical simulations give the fixed-point linear ($(x_0, x_0/\beta)$) stability as a function of I_{ext} and the pump strength α when $\beta = 0.3$, as shown in Fig.2(a). The stability of those fixed points depends on $Re(\lambda_i^+)$, these fixed points become unstable when $Re(\lambda_i^+) > 0$. However, the eigenvalues would become complex conjugated when $T^2 - 4\Delta < 0$. Hence, we mark $Re(\lambda_i^+) = 0$ and $T^2 - 4\Delta = 0$ in Fig.2(a), respectively. Then, the time evolution and the oscillation phase space of those fixed points in the regions 2 and 3 are shown in Fig.2(b)(c) and Fig.2(d)(e), respectively. Under a small disturbance of I_{ext} , the system reciprocates on a limit cycle. And the system will shrink to a stable focus under a large I_{ext} .

The spiking behavior of single neurons can be achieved by controlling the parameter I_{ext} . When I_{ext} increases, the amplitude of neuron pulses gradually decreases. However, for the increment of I_{ext} to a certain value, the neuron pulses will no longer appear, as shown in Fig.2(f). This process is consistent with the evolution direction of the arrow indicated by Fig.2(a), that is, the system appears Andronov-Hopf (AH) bifurcation with the increase

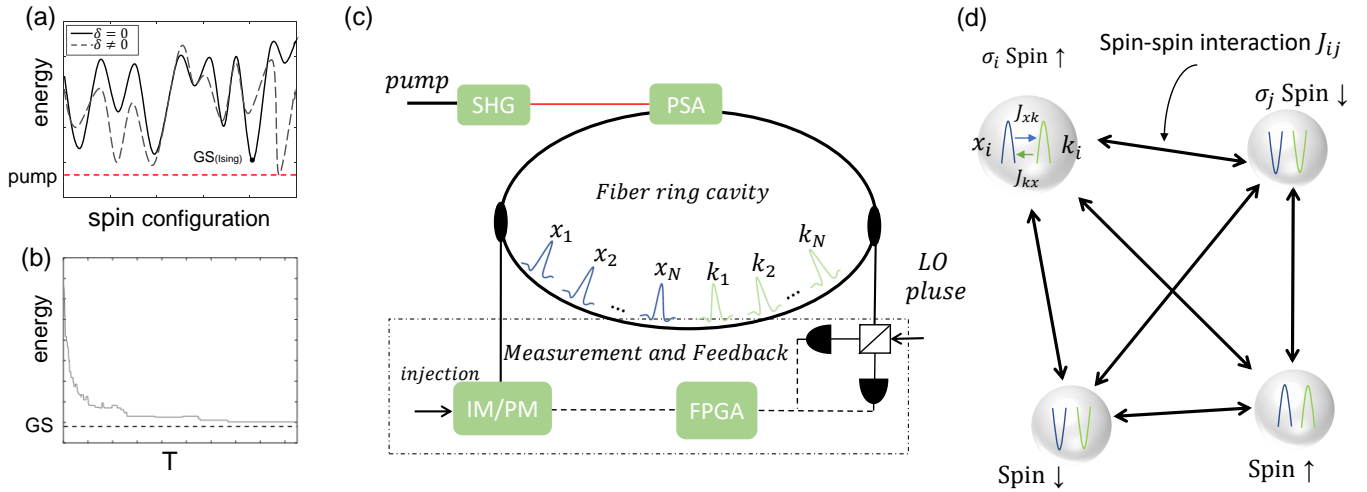


FIG. 1. Schematic diagram of SNN-CIM. a. Variation of energies with spin configuration for homogeneous and inhomogeneous spin amplitudes. The red line is the pump intensity, which does not excite the correct ground state spin configuration. b. The time evolution of the energy, due to the amplitude heterogeneity, is frozen in the excited state. The dashed line is the ground state energy. c. Optical implementation of SNN-CIM. The pump is turned on to generate type-x DOPO, and when it is turned off, the modulation generates type-k pulses. d. Spiking neural network. IM: intensity modulator, PM: phase modulator, SHG: second harmonic generation, PSA: phase sensitive amplification, FPGA: field programmable gate array.

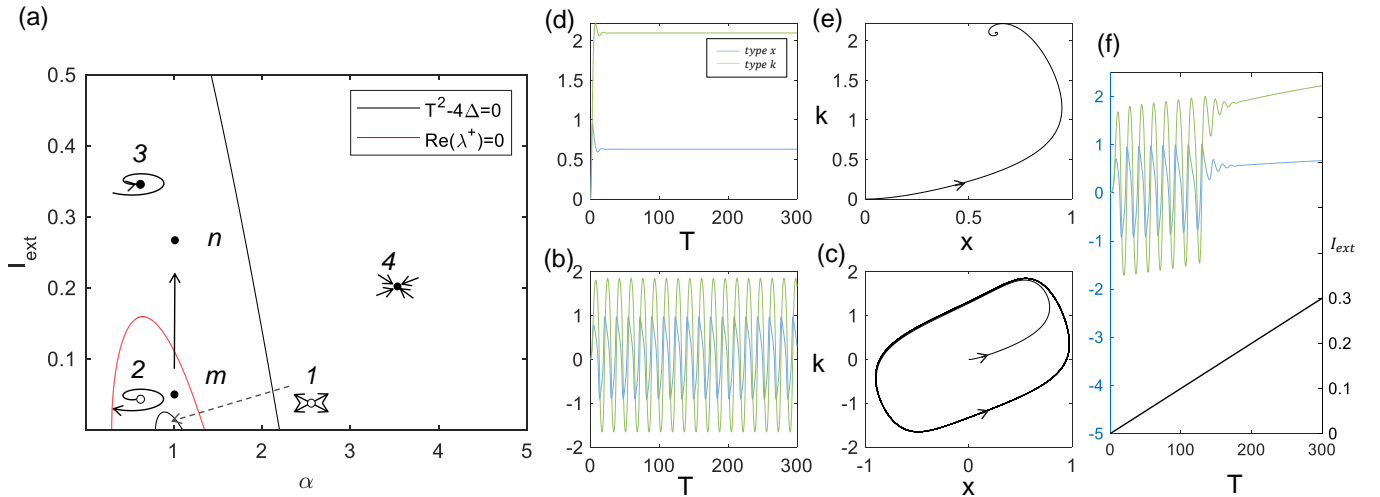


FIG. 2. Dynamic behavior of spiking neurons. a. The effect of pump strength α and I_{ext} on the stability of the fixed point. $\beta = 0.3$. b. and c. The time evolution and phase space trajectories of the type-x DOPO pulse and type-k pulse at point m in (a), $\alpha = 1$ and $I_{ext} = 0.05$. d. and e. Corresponding to n points, $\alpha = 1$ and $I_{ext} = 0.25$. f. The time evolution of the type-x DOPO pulse and type-k pulse with the increase of I_{ext} .

of I_{ext} , which make the fixed points change from an unstable limit cycle to a stable focused point. This proves that the optical pulse network has the properties of the class-II neurons by antisymmetrically coupling a pair of nonlinear gain DOPO pluse and dissipation optical pluse.

In addition, as shown in Fig.2(g), we find a smaller I_{ext} could exhibit a larger firing rate by taking a Fourier transform of the temporal evolution of neurons under different I_{ext} . For the Ising model with antiferromagnetic coupling, the evolution of the energy $E_{Ising} = -\sum_{ij} \sigma_i \sigma_j / 2$ is

accompanied by an amplification of the coupling term. In this model, I_{ext} corresponds to the coupling term on the i th spin, that is, the firing rate decreases (I_{ext} increases) during the evolution of the Ising model. Moreover, the cluster neurons can also be synchronized to a low firing rate.

C. Instability of the local Minimum and SNN-CIM Algorithms

Similar to the analysis of the linear stability of pump and I_{ext} on the fixed points, Fig.3(a) shows the effect of dissipation β and I_{ext} on the linear stability of those fixed points. Those fixed points that freeze at local minima tend to be located in region 3. The stability of the local minima can be influenced to escape from the frozen local minima by adjusting the dissipation and coupling strength. To overcome the local minima and make the system to escape from the frozen state, we choose $Re(\lambda_i^+) > 0$ by reducing the dissipation β and coupling strength ϵ which forces these fixed points into region 2 to destabilized. And then, the system continues to search for the ground state with lower energy by gradually increasing the coupling strength.

To give an example of the algorithm, we apply the SNN-CIM algorithm on the MAX-CUT problem of G1.

In Fig.3(b), the time evolution of the type- x DOPO and type- k pulses, the energy and the number of cuts of the system are given. Specifically, if the energy is frozen in a local minima state, we tend to reduce β which makes the system unstable. Then, there is fluctuation of the energy and the system continues to search for the lower energy state. Finally, if the system energy is higher than the lowest energy before this moment, as in Fig. 3, the optimal solutions could be obtained as $edges = 11624$ near $T=1350$, after that the system will be unstable until another lower energy is searched.

D. The performance of SNN-CIM Algorithm on MAX-CUT Problem

Here in this part, we describe the performance of SNN-CIM algorithm on the Max-Cut problem, and then compare with other types of computing devices such as those based on simulated annealing and conventional CIM. We discuss the performance of these investigated devices on different size of the Ising problems.

We choose the simulated annealing (SA) algorithm and the SNN-CIM algorithm on the G1-G21 graph of 800 nodes, and the G22-G42 graph of 2000 nodes, and also compared the performance with the conventional CIM and the CIM with sigmoid function optimization in Ref.[23].

The performance of the computational results are shown in Fig.4. Here we choose the relative error $\Delta C = 100(1 - C/C_{opt})$ of the optimal value during 50 runs as the result, and C_{opt} denotes the best-known value reported in literature. In the 800 nodes problem, CIM with sigmoid function and SNN-CIM often find the solutions very close to the optimal value, while the performance of the SA and CIM are relatively poorly. And, the mean values of the relative errors of SNN-CIM and CIM with sigmoid function in the optimal value of G1-G21 are 0.3%

and 0.4%, respectively. The performance of SNN-CIM is slightly better than that of CIM with sigmoid function. Under the more complex 2000-node problem, SNN-CIM is significantly closer to the optimal value than the other three algorithms. In addition, for more complex problems with random connectivity and non-uniform node degrees (G39,G40,G41,G42), SNN-CIM with unstable local optima can also achieve better computational performance. This shows that SNN-CIM will have more potential in more complex combinatorial optimization problems.

The computational performance of the SNN-CIM algorithm on GSET is also shown in Table.1, which is compared with SA and CIM. We note that the algorithm of SNN-CIM has an unparalleled advantage in computing time to find suboptimal but adequate solutions for the application, both in the time and accuracy of the solutions. Based on the above analysis, our proposed SNN-CIM has excellent performance on combinatorial optimization problems.

III. CONCLUSION

In addition, the model can be implemented by adding dissipative pulses to the existing CIM based on fiber ring cavity, which is expected to improve its computational performance and solve the problem of freezing in the excited state during the calculation process. By using integrated photonics direct coupling and high repetition frequency lasers, it is expected to increase the pulse firing rate and the number of neurons, improve computing power, and provide a better simulation platform for spiking neural networks. Finally, the use of the sigmoid function for the coupled term response in this model, which is widely used in neural networks, creates an interesting connection between CIM and neuromorphic computing, with the potential to excite the research in the perceptron and pattern recognition of fiber-rings cavity based CIM.

IV. ACKNOWLEDGEMENT

This research was funded by the National Natural Science Foundation of China (Grants Nos. 62131002, 62071448), and the Fundamental Research Funds for the Central Universities (BNU).

V. DATA AVAILABILITY

The GSET instances used for the tests is available at <https://web.stanford.edu/~yyye/yyye/Gset/>. The SA algorithm temperature adjustment is based on a logarithmic function, $T = T_0 \log_2(1 + t_0/t)$. All programs are written by matlab and run on intel i7-10700F 2.9GHz.

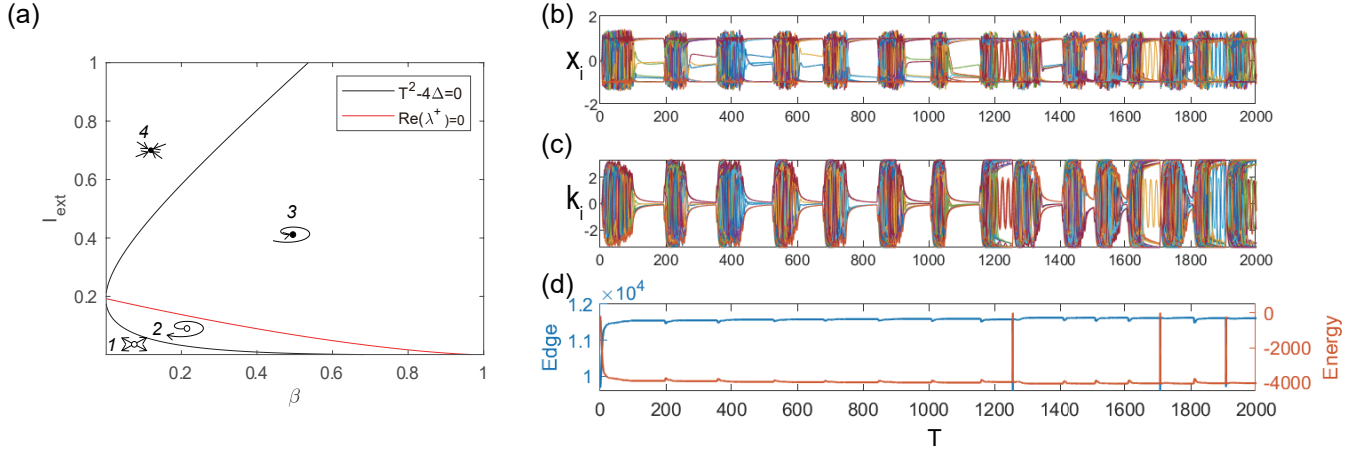


FIG. 3. SNN-CIM solves the MAX-CUT problem of G1. a. The effect of β and I_{ext} on the stability of the fixed point. $\alpha = 1.0$. b. Evolution of type- x DOPO pulse amplitude with calculation time. c. Evolution of type- k pulse amplitude with calculation time. d. Energy and number of cuts as a function of computation time.

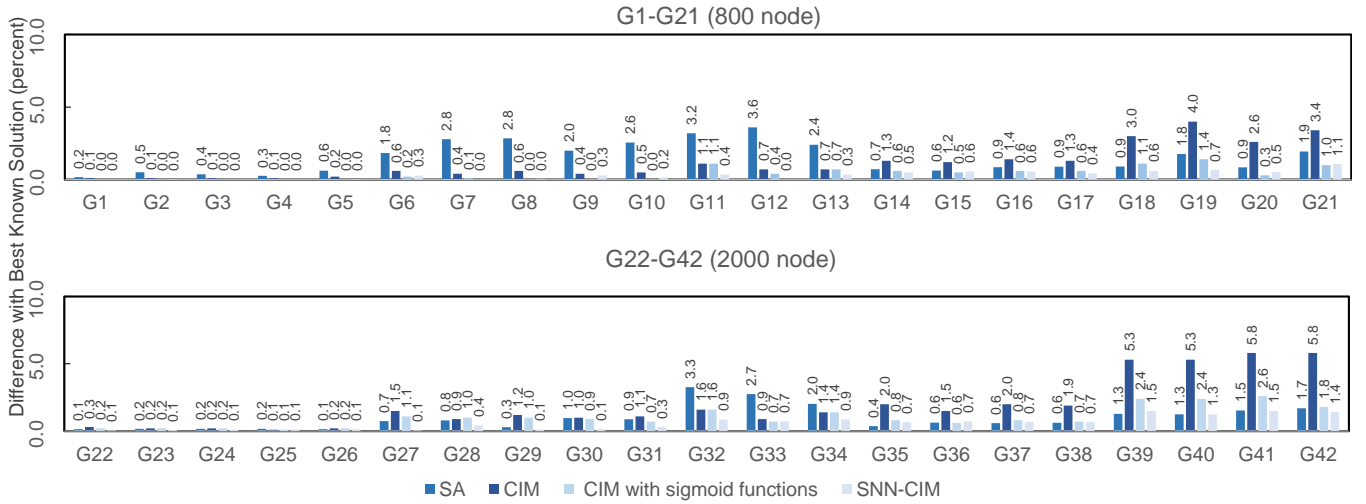


FIG. 4. Computational performance of the SNN-CIM algorithm on the MAX-CUT problem for a given problem. a. Relative error of the optimal value of simulated annealing algorithm, CIM, CIM with sigmoid function, and SNN-CIM for 50 runs on the MAX-CUT problem of a graph with 800 nodes. b. More complex 2000 node situation.

- [1] D. B. Kitchen, H. Decornez, J. R. Furr, and J. Bajorath, *Nature reviews Drug discovery* **3**, 935 (2004).
- [2] A. Soler-Dominguez, A. A. Juan, and R. Kizys, *ACM Computing Surveys (CSUR)* **50**, 1 (2017).
- [3] F. Barahona, M. Grötschel, M. Jünger, and G. Reinelt, *Operations Research* **36**, 493 (1988).
- [4] S. Arora and B. Barak, *Computational complexity: a modern approach* (Cambridge University Press, 2009).
- [5] T. Kadowaki and H. Nishimori, *Physical Review E* **58**, 5355 (1998).
- [6] A. Das and B. K. Chakrabarti, *Reviews of Modern Physics* **80**, 1061 (2008).
- [7] Z. Wang, A. Marandi, K. Wen, R. L. Byer, and Y. Yamamoto, *Physical Review A* **88**, 063853 (2013).
- [8] B. Sutton, K. Y. Camsari, B. Behin-Aein, and S. Datta, *Scientific reports* **7**, 1 (2017).
- [9] M. Saccone, F. Caravelli, K. Hofhuis, S. Parchenko, Y. A. Birkhölzer, S. Dhuey, A. Kleibert, S. Van Dijken, C. Nisoli, and A. Farhan, *Nature Physics*, 1 (2022).
- [10] R. Hamerly, T. Inagaki, P. L. McMahon, D. Venturelli, A. Marandi, T. Onodera, E. Ng, C. Langrock, K. Inaba, T. Honjo, *et al.*, *Science advances* **5**, eaau0823 (2019).
- [11] A. Marandi, Z. Wang, K. Takata, R. L. Byer, and Y. Yamamoto, *Nature Photonics* **8**, 937 (2014).

TABLE I. Computational performance of SA, CIM, and SNN-CIM on GSET. TTS is time-to-solution of reach 98 percent of the best solution. The optimal solutions for SA, CIM and SNN-CIM are obtained under 10, 50 and 50 runs, respectively. Values in parentheses indicate that the results of TTS_{98} cannot be obtained, and are replaced by TTS_{95} . The best maximum cuts known from Ref.[34]

| ID | N | J_{ij} | Edge | C_{opt} | C_{SA} | C_{CIM} | $C_{SNN-CIM}$ | $TTS_{SA}(s)$ | $TTS_{CIM}(s)$ | $TTS_{SNN-CIM}(s)$ |
|----|------|---------------|-------|-----------|----------|-----------|---------------|---------------|----------------|--------------------|
| 1 | 800 | {0, 1} | 19176 | 11624 | 11604 | 11597 | 11624 | 16.1514 | 3.8065 | 0.0373 |
| 6 | 800 | {0, ± 1 } | 19176 | 2178 | 2138 | 2149 | 2172 | 20.4624 | 4.0332 | 1.3423 |
| 11 | 800 | {0, ± 1 } | 1600 | 564 | 546 | 550 | 562 | (8.46337) | (0.4107) | 0.4775 |
| 14 | 800 | {0, 1} | 4694 | 3064 | 3042 | 2993 | 3049 | 11.9894 | (1.8703) | 0.0786 |
| 18 | 800 | {0, ± 1 } | 4694 | 992 | 983 | 942 | 986 | 20.4379 | (8.418) | 1.52 |
| 22 | 2000 | {0, 1} | 19990 | 13359 | 13340 | 13279 | 13352 | 2169.69 | 14.048 | 0.9654 |
| 27 | 2000 | {0, ± 1 } | 19990 | 3341 | 3316 | 3271 | 3339 | 2760.23 | (23.568) | 27.768 |
| 32 | 2000 | {0, ± 1 } | 4000 | 1410 | 1364 | 1364 | 1398 | (2909.38) | (7.1411) | 32.101 |
| 35 | 2000 | {0, 1} | 11778 | 7684 | 7656 | 7448 | 7634 | 1644.46 | (14.806) | 1.2013 |

- [12] T. Inagaki, K. Inaba, R. Hamerly, K. Inoue, Y. Yamamoto, and H. Takesue, *Nature Photonics* **10**, 415 (2016).
- [13] P. L. McMahon, A. Marandi, Y. Haribara, R. Hamerly, C. Langrock, S. Tamate, T. Inagaki, H. Takesue, S. Utsunomiya, K. Aihara, *et al.*, *Science* **354**, 614 (2016).
- [14] T. Inagaki, Y. Haribara, K. Igarashi, T. Sonobe, S. Tamate, T. Honjo, A. Marandi, P. L. McMahon, T. Umeki, K. Enbutsu, *et al.*, *Science* **354**, 603 (2016).
- [15] T. Honjo, T. Sonobe, K. Inaba, T. Inagaki, T. Ikuta, Y. Yamada, T. Kazama, K. Enbutsu, T. Umeki, R. Kasahara, *et al.*, *Science advances* **7**, eabh0952 (2021).
- [16] Fabian, Bhm, Guy, Verschaffelt, Van, der, and Sande, *Nature communications* **10**, 3538 (2019).
- [17] Q. Cen, T. Hao, H. Ding, S. Guan, Z. Qin, K. Xu, Y. Dai, and M. Li, *arXiv preprint arXiv:2011.00064* (2020).
- [18] D. Pierangeli, G. Marcucci, and C. Conti, *Physical Review Letters* **122**, 213902 (2019).
- [19] Y. Fang, J. Huang, and Z. Ruan, *Physical Review Letters* **127**, 043902 (2021).
- [20] W. Sun, W. Zhang, Y. Liu, Q. Liu, and Z. He, *Optics Letters* **47**, 1498 (2022).
- [21] Y. Okawachi, M. Yu, J. K. Jang, X. Ji, Y. Zhao, B. Y. Kim, M. Lipson, and A. L. Gaeta, *Nature communications* **11**, 1 (2020).
- [22] T. Leleu, Y. Yamamoto, S. Utsunomiya, and K. Aihara, *Physical Review E* **95**, 022118 (2017).
- [23] F. Böhm, T. V. Vaerenbergh, G. Verschaffelt, and G. Van der Sande, *Communications Physics* **4**, 1 (2021).
- [24] S. Reifenstein, S. Kako, F. Khoystate, T. Leleu, and Y. Yamamoto, *Advanced Quantum Technologies* **4**, 2100077 (2021).
- [25] T. Leleu, Y. Yamamoto, P. L. McMahon, and K. Aihara, *Physical Review Letters* **122**, 040607 (2019).
- [26] S. Kako, T. Leleu, Y. Inui, F. Khoystate, S. Reifenstein, and Y. Yamamoto, *Advanced Quantum Technologies* **3**, 2000045 (2020).
- [27] T. Leleu, F. Khoystate, T. Levi, R. Hamerly, T. Kohno, and K. Aihara, *Communications Physics* **4**, 1 (2021).
- [28] T. Inagaki, K. Inaba, T. Leleu, T. Honjo, T. Ikuta, K. Enbutsu, T. Umeki, R. Kasahara, K. Aihara, and H. Takesue, *Nature communications* **12**, 1 (2021).
- [29] W. Maass, *Neural networks* **10**, 1659 (1997).
- [30] R. Brette, M. Rudolph, T. Carnevale, M. Hines, D. Beeman, J. M. Bower, M. Diesmann, A. Morrison, P. H. Goodman, F. C. Harris, *et al.*, *Journal of computational neuroscience* **23**, 349 (2007).
- [31] E. M. Izhikevich, *IEEE Transactions on neural networks* **14**, 1569 (2003).
- [32] V. Mnih, K. Kavukcuoglu, D. Silver, A. A. Rusu, J. Veness, M. G. Bellemare, A. Graves, M. Riedmiller, A. K. Fidjeland, G. Ostrovski, *et al.*, *Nature* **518**, 529 (2015).
- [33] Q. Yu, K. C. Tan, and H. Tang, in *The 2012 International Joint Conference on Neural Networks (IJCNN)* (IEEE, 2012) pp. 1–7.
- [34] F. Ma and J.-K. Hao, *Annals of Operations Research* **248**, 365 (2017).